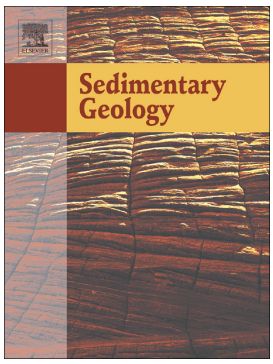


# Processes of MISS-formation in a modern siliciclastic tidal flat, Patagonia (Argentina)

Lucía Maisano, Diana G. Cuadrado, Eduardo A. Gómez

PII: S0037-0738(18)30270-7
DOI: https://doi.org/10.1016/j.sedgeo.2018.12.002
Reference: SEDGEO 5423

To appear in: *Sedimentary Geology*

Received date: 18 September 2018
Revised date: 11 December 2018
Accepted date: 13 December 2018

Please cite this article as: Lucía Maisano, Diana G. Cuadrado, Eduardo A. Gómez , Processes of MISS-formation in a modern siliciclastic tidal flat, Patagonia (Argentina). Sedgeo (2018), https://doi.org/10.1016/j.sedgeo.2018.12.002

# Processes of MISS-formation in a modern siliciclastic tidal flat, Patagonia (Argentina)

Lucía Maisano*, Diana G. Cuadrado and Eduardo A. Gómez

Instituto Argentino de Oceanografía (IADO, CONICET), Florida 7500, Bahía Blanca (8000), Provincia Buenos Aires, Argentina

Departamento de Geología, Universidad Nacional del Sur, San Juan 670, Bahía Blanca (8000), Provincia Buenos Aires, Argentina

*Corresponding author at: IADO-CONICET, 8000-Bahía Blanca, Argentina. Fax: +54 291 4861519.

E-mail address: lulamaisano@gmail.com



## ABSTRACT

The study focus on the description of several MISS as erosional pockets and remnants, flipped-over edges, and large microbial deformation structures as roll-ups, folds and gas domes, in the context of sediment composition, hydraulics, and geomorphology. The aim of the paper is to recognize the mechanisms of formation of MISS by analyses on hydrodynamics under the influence of the geomorphology.

The study was conducted in an elongated inactive tidal channel colonized by microbial mats (2.5 x 0.3 km) in a progradation environment. To continuously record the water-

level fluctuations, a HOBO water level logger was placed 40 cm below the flat surface for two years. The sea water enters several times a year, during storms, where the flood currents were characterized by faster velocity than ebb currents, reaching a water depth up to 0.70 m over the tidal flat. That coastal process creates MISS over the tidal flat.

The most conspicuous microbial structures are the huge deformation roll-ups several m-scale, associated to elongated rip-off mats, folds and flipped over mats. The process of fluidization was postulated to explain the sand-infilling of gas domes and folds we observed. This process would result from the wave action on the water column that produces a temporal fluid behavior of the underlying sand.

**Keywords:** tidal currents; roll-up mat structure; fold mat structure; liquefaction; geomorphology.

## 1. INTRODUCTION

Microbial mats are constituted by organic colonies which grow originally on water-sediment interface as thin biofilms which may evolve, under favourable conditions, to a thick laminated layer forming a cohesive and leathery carpet in several square kilometre extensions (Gerdes et al., 2000; Kremer et al., 2008; Noffke, 2010; Stal, 2012). Studies on microbial mat structures are well known from carbonate environment (Chafetz and Buczynski, 1992; Andres and Reid, 2006), while microbial mat influence on clastic sediments has received increasing attention in recent years (Schieber, 1999). In fact, the primary sedimentary structures in a siliciclastic sedimentary environment formed by the interaction of microbial mats with physical dynamics have received the particular name of MISS (microbially induce sedimentary structures, *sensu* Noffke et al., 2001).

Biostabilization protects sedimentary surface against erosion (Noffke and Paterson, 2008) and some structures arise from this process such as gas domes, erosional pockets, roll-ups structures (Noffke, 2010). Gas domes derive from intra-sedimentary gas pressure producing a flexible deformation of biofilm or microbial mat (Noffke, 2010). The different gaseous compounds such as $O_2$, $CO_2$ and $CH_4$ are produced by microbial activity, photosynthesis and decomposition (Gerdes et al., 2000, Schieber, 2004). Gas domes were described in several tidal flats; in turn Bose and Chafetz (2011) found them occurring in the upper supratidal areas in a microtidal regime. Also, Gerdes (2007) and Noffke et al. (2008, 2010) described the presence of gas domes in different environments, not restricted to arid areas but occur on tidal flats of temperate humid climate zone and also subaquatically. Noffke (2010) associated gas domes with the normal high water line due to the pushing of gases by the rising tide.

Bose and Chafetz (2011) related the formation of erosional pockets, mat chips, ripped-up mats, and eroded boundaries of mats to physical destruction process indicating a high energy environmental condition for their development in a micro tidal environment. Also, Noffke (1999) described erosional pockets and remnants in tidal flats of Mellum Island where the sandy surface of the pockets were not overgrown by microbial mats exposing ripple marks.

As a consequence of erosion due to currents sufficient strong over cohesive mats, flipped-over edges or deformed roll-up fragments can be formed (Schieber, 2004). In relation with their genesis, roll-up structures were defined by Noffke (2010) recognizing two types; one is related to the curled edges of mat chips up to 5 cm-in diameter. The second type includes larger mat pieces of several meters rolled up by storm bottom currents, sometimes related to enormous strength. A unique study has mentioned huge

roll-up mat pieces (several $m^2$ in size) rolled by strong storm currents in Portsmouth Island (USA), after a post-hurricane phenomena in 2003 (Noffke, 2010).

We documented several enlarged MISS in a supratidal flat at Paso Seco (Argentina) where high dimensions are the most conspicuous feature, especially in microbial roll-ups, mat folds and gas domes. The environment is an elongated evaporitic-siliciclastic system, where recently hydrodynamic measurements enhance a previous study (Cuadrado et al., 2015) and provide more new evidence about mechanical explanations for their formation. The aim of the paper is to describe the interaction of biostabilized microbial mats with hydraulics, recognizing the mechanisms of formation and emphasizing the geomorphologic control as an important factor to take into consideration. In fact, the paper offers new understanding on Earth processes where biology, physics, sedimentology, and geomorphology are closely intertwined.

## 2. STUDY AREA

Paso Seco is located in northern Patagonia in Argentina (40°33′S; 62°14′W; Fig. 1). The climate corresponds to semiarid temperate of the Meseta (Iglesias, 1981), characterized by an average annual rainfall < 300 mm and where the potential evaporation commonly exceeds precipitation (Ferrelli et al., 2012). In spite of its mid latitude and temperate condition, aridity is common in the study area, and due to continual seawater inundation the formation of a saline system is developed. Calcium carbonate, gypsum and halite are commonly precipitate on the tidal flat as remnants of evaporative processes.

Geomorphologically, the study area is an inactive tidal channel that has been choked by a sand spit formed by NE longshore sediment transport along the coast, as a result of progradation processes. As a consequence, the bottom of the ancient tidal channel is nowadays a long exposed tidal flat. The large elongated area, SW-NE (226°)

orientation, comprises 3.5 x 0.4 km widespread surface colonized by microbial mats (Fig. 1A). The coastal tidal range is mesotidal, where the mean and maximum tidal ranges are 1.62 m and 2.5 m, respectively. The area is eventually flooded by seawater when meteorological and oceanographic conditions act simultaneously: severe storm with strong winds, and high waves under spring tides. When wave height overpass 2 m and the sea level exceed the sand spit, the sea water enters into the inactive channel (Fig. 1B).

The tidal flat is colonized by a dominant mat group non-heterocystus, trichome-forming cyanobacteria, such as *Microcoleus chthonoplastes* (Cuadrado and Pan, 2018) which is the main constructor of epibenthic mats that secretes large amounts of EPS. The epibenthic mat makes a firm sedimentary surface.

## 3. METHODS

The study includes measurements of hydraulic process over two-year period when MISS were documented during field visits. To record the tidal flooding over the flat and water-level fluctuations in the water table, a HOBO water level logger (Onset-model U20; 2.5 cm diameter, 15 cm length) was deployed into a vertically buried, perforated PVC pipe, 40 cm in depth to remain submerged as long as possible. The bottom of the pipe was covered by a permeable textile. The sensor registered water level and temperature every 10 min and the measurements were conducted from March 2015 to March 2017. The water level data were corrected by atmospheric pressure by means of another logger placed in an upper level close to the tidal flat. Sedimentary cores (inner diameter = 8.5 cm; height = 20 cm) were taken from the flat to document the microbial sedimentary profile. On a field trip after a storm, images and photographs were obtained

from an UAV (Karma® unmanned aerial vehicle) holding a GoPro 5 camera to document the microbial structures covering the large area.

## 4. RESULTS

### *4.1. Hydrodynamic conditions*

Several high-energy floodings (more than 50 cm water column height in less than 4 h) over the colonized sediments were recorded throughout the two years of study (Fig. 2A). The average inundation is 43 times per year and the water temperature fluctuates between 6°C in winter to 29°C in summer. The flooding presents the same pattern during the year, a fast increase in water column over the surface associated to a flood tide, and a subsequent gradual decrease associated to ebb tide. Some characteristics of the flooding are documented in the following. In the period between March 20$^{th}$ and April 25$^{th}$ 2015 (early autumn) there were three flooding over the microbial flat characterized by different features (Fig. 2B). The first one, which occurred on March 20$^{th}$, reached the highest water column of 0.45 m over the tidal flat sharply in 1 h, decreasing down during ~24 h, being maintained later the water level near the mat surface during 6 days (Fig. 2C). After that, the water level drops off forming an aquifer below the surface tidal flat where the water table reached 0.25 m depth during 5 days until the next inundation occurred. Interesting to point out that before this inundation, the water table was 0.30 m deep.

The second flooding event occurred April 1$^{st}$ (Fig. 2D). In less than 2 h the water column increased over the flat reaching 0.25 m. After the maximum height of the water column was reached, the water drained the tidal flat over the course of 4 hours, maintaining the water table near the surface during four days. After several days a rainfall event replenished the aquifer (up to the surface) which lasted for 4 days until the

third flood took place (pointed by an arrow in Fig. 2B). On April 20th, in coincidence with a field trip, there was a sea-flooding (the third inundation) which reached 0.20 m over the tidal flat in less than 1 h and the seawater remained over the tidal flat for nearly 4 h, flowing off by more than 4 h (Fig. 2E). The surficial current velocity measured proximate the maximum water column (pointed by an arrow in Fig. 2E) was 0.50 m $s^{-1}$.

A high flooding was observed in May 2015 when the inundation led to a ~0.55 m of water column over the tidal flat in 3.5 h (Fig. 2F), gradually decreasing the water level during ebb for 27 h. After that, there were four lower peaks every 12 h during the two following days with heights between 0.05 and 0.15 m. These minor peaks would be related to tidal fluctuations. The ratio H/T is proportional to the current velocity; therefore it can be inferred from the records that the flood current velocity is always higher than the ebb one.

It is important to notice that the water table in austral winter (June-September) remains near the surface for long time (days to months). In June 2015, after a flooding, the seawater remained on the tidal flat during 25 days (Fig. 3A). During this time, there were several flooding superposed, reaching a water column height between 0.10 and 0.50 m. Interesting, the highest water column on June 17th was maintained fluctuating during 8 h due to wind driven waves (arrow in Fig. 3A). Moreover, in June 2016, the seawater flooded over the surface and was maintained over the tidal flat for more than two months including several floodings (Fig. 3B). In contrast, during summer the tidal flat remains dry exposing to the solar radiation for several days. The water table varied within the aquifer and commonly its level rose with the high tide. In November-December 2015 when the mat tidal flat was aerially exposed for 47 days, the water table varied between near the surface and 0.30 m deep (Fig. 3C). Similarly, in January-February 2017 the water table dropped reaching the maximum depth of 0.50 m under

the tidal flat, increasing with high tide (Fig. 3D). Sometimes the sea water income was intra sedimentary and others it overwhelmed the tidal flat.

*4.2. Seasonal appearance and character of the microbial tidal flat*

Field surveys observed a diverse mat surface appearance during different seasons. In July 2015 (austral winter) the tidal flat showed large detached mat fragments spread atop the vegetation (Fig. 4A) as a consequence of a previous inundation occurred in May, when the highest water level was recorded this year (see Fig. 2F). Also, fragments of mat were found at the vegetated fringe of the area, pointing out the water level height that reached the area (Fig. 4B, C). The tidal flat remained covered by a thin seawater layer during winter due to the low evaporation and the position of the ground water table close to the sedimentary surface (Fig. 4D). During summers, the most intense solar radiation and high temperatures increases evaporation and dries the mat covered surface out (Fig. 4E). Desiccation erodes and halite crystals form. However, the mat remained moist underneath the surface (Fig. 4F).

*4.3.Microbial mat characteristics*

The main characteristic of the microbial mat in the study zone is its thickness, which varies from 0.5 to 1.5 cm (Fig. 5A). Under wet condition the mat can be easily separated from the underlying silty sand layer (thickness > 2 cm) and exposed high cohesiveness and plasticity under wet condition. This makes the mat coherent and soft with a flexible nature that allows the generation of deformation structures in response to an increase in shear stress. They form a leathery surface merging high mechanical strength with very low permeability, which prevent the escape of gas to atmosphere, forming mat domes that separate the microbial mat from the underlying sediment as was

documented by Noffke (2010). Contrarily, under dry conditions during subaerial exposure of the tidal flat, the upper microbial mat shrinks in a greater extent than the underlying sandy layer, forming desiccation cracks with a polygonal pattern. Sometimes, the edges can also curl up due to differential layers shrinkage. The low permeability protects the underlying sediment from the water loss, being a barrier between the substratum and the atmosphere (Fig. 4F).

### *4.4. Microbially induced sedimentary structures (MISS)*

Several MISS were found in the tidal flat of Paso Seco.

*Gas Domes.* This structure usually takes a circular shape in horizontal plane. The domes present different diameter sizes, between 1 cm to 20 cm (n= 25) in diameter. Most of the major features were identified during the inundation of the tidal flat, showing their surface above the water level (Fig. 6A), maintaining their morphology during dry condition (Fig. 6B). They often show a hollow between the surface mat and the underlying sediment (Fig. 6C), but occasionally the underlying sandy sediment exhibit the same dome shape of the surficial mat displaying convex bedding planes (Fig. 6D).

*Flipped-over edges.* They are formed when a mat ruptured and the fragment is bended with an upturn of 180° resting on the surficial microbial mat. This structure can develop as isolated features along tears leaving the underlying sediment exposed (Fig. 7A). Several flipped-over structures are found showing different direction, however, sometimes they were found in association to desiccation cracks whose edges were bended in an ebb direction (Fig. 7B).

*Mat Folds.* A mat fragment detached from the underlying sediment slide over the underlying sediment creating a fold (Fig. 8A). Several folds were mainly formed parallel to each other with variable axial plane. Also, recumbent folds can be seen where

the fold axial plane is oriented at low angle with the horizontal tidal flat (Fig. 8B). The length of the feature depends on the fragment size that was ripped-up and slide over the underlying layer, varying from 15 cm to more than 1 m. Interesting to mention, the underneath sediment sometimes presents the same shape than the surficial mat (Fig. 8C).

*Microbial Roll-up.* This feature consists of surficial mat fragment rolled over some distance after being ripped-up and detached from the substrate (Fig. 8D). It is made up of a very flexible mat with ~1 cm thickness. The number of twist of the rolled-mat differs from one feature to other, depending on the length of the ripped mat. The structure size has reached up to ~ 2 m in length and ~ 25 cm in height forming thick overwhelmed elliptical bodies (Fig. 8E). This elliptical shape probably depends on the thickness of the underlying sediment attached to the mat and the weight of the structure.

*Erosional pockets and remnants* (*sensu* Noffke, 1999). After strong storms the microbial mat can be mechanically destroyed forming a rounded to elongate depression, the erosional pocket, characterized by a rippled bottom. They were more than 1 m-length. The relic mat that protects the elevated surface raises several cm-heights (2-3 cm). These structures were found near the southern margin of the area.

*4.5. Relation between hydrodynamics and MISS*

After a storm characterized by strong winds (>50 km $h^{-1}$) during winter 2018 (June 23$^{th}$), the area was documented by means of a UAV. Large microbial deformation structures were identified especially large mat roll-ups in association with microbial folds and flipped-over mats (Video 1, Apendix A). Two days before the field survey, the inundation reached the maximum water column ever recorded, 0.67 m (in less than 90 min) over the tidal flat level (Fig. 9A). Once the highest peak of flooding diminished

to 0.5 m-water depth, the water level was maintained during 6 h over the microbial flat showing fluctuation of ± 0.05 m due to wind waves. During the field trip the flat exhibited large erosional pockets with different forms and sizes (between 3 to 8 m; Fig. 9B), extensive mat tears (between 2 to more than 8 m) in the longitudinal channel direction (Fig. 9C) ending in large roll-ups with different sizes (Fig. 9D, E). Moreover, after the creation of tears, the surficial mat slipped over the underlying sediment forming folds (Fig. 9F, G). The borders of the broken mat in the tears sometimes folded over perpendicularly to the stripped mat (Fig. 9F). Meanwhile roll-ups structures and stripped mats always have been created by a mean flood direction (Fig. 10), both mat folds and flipped-over edges have different directions (Fig. 9F, G). The uncohesive underlying sediment that had been exposed by the broken mat was transported along the tidal flat over the mat (ST in Fig. 10C). During the following field trip carried one month later (August 9$^{th}$) the mechanism of formation was clearly identified by document the position of the mat structures over the flat in relation to hydrodynamic conditions (Fig. 11).

## 5. DISCUSSION

### *5.1.Role of the epibenthic mats and recolonization effect*

The tidal surface is overgrown by epibenthic microbial mats, which are typical in supratidal zones (Noffke 2010). In the present study, cyanobacteria *Microcoleus chthonoplastes* which is the main constructor of epibenthic mats, secretes large amounts of EPS as a protection against desiccation when the tidal flat is exposed (Decho and Gutierrez, 2017). Such fact also contributes to make a slippery mat surface reducing the frictional forces of the flow and protecting the underlying sandy layers from erosion by moderate currents, and only strong currents can damage them (Noffke, 2010). The

recolonization occurs during calm conditions after the storm (Noffke, 2010). The appearance of yellow-brownish hue and very small photosynthetic bubbles ~1 mm in a few centimeters of water suggests recolonization of barren areas by heavy evolving biofilm (Pan et al., 2017; Fig. 12A). Wet flipped-over structure may present a reticulate surface as a new mat growth (Fig. 12B), producing polygonal geometric shapes (Bose and Chafetz, 2009). Probably, the wet medium gives the capacity for the filamentous cyanobacteria to migrate and eventually form reticules also along the edges similarly to shallow depressions documented by Cuadrado and Pan (2018). The amalgamation of the microbial structure with the sedimentary surface is probably the first stage before developing a laminar leveling surface by the growth of epibenthic mat (Noffke, 2010). Consequently, the recolonization that occurs after each inundation makes also the deformation structures edges to be erased (Fig. 12C), forming a new sedimentary layer including the microbial structure into the sedimentary sequence. Figure 13A exposes a biolaminite in the erosional flank of a tidal creek revealing small gas domes or mat folds, similar to that observed on the surface of the tidal flat (Fig. 13B). Those structures can be associated to a deformation structure identified 13 cm in depth in a vertical cross-section of a sedimentary core (Fig. 13C) which was capped by newer microbial mats.

*5.2. Initial MISS formation*

One of the effects of seawater flooding is the replenishment of the aquifer that makes the pore-sediment air moving to the surface making the mat domes formation (Noffke, 2010) and the separation of the surficial mat from the underlying sediment. The funneled sea-water enters the study area forming fast currents due to the morphology. The water turbulence depends on the energy level of the storm winds. Slow currents

(0.5 m $s^{-1}$) under weak winds may easily uplift ripped fragment of the microbial carpet from the underlying sediment due to the action of the shear stress over the bottom (Video 2, Appendix A). However, severe storms characterized by a high water depth might act over the microbial mat during several hours (e.g., 0.65 m during 6 hs, winter 2018, Fig. 9A) in association to wind wave action (variation $\pm$ 5 cm in the water surface).

Noffke (2010) has quantified the shear stress needed for initial erosion of epibenthic mats and found values 9 times higher than initial erosion of sterile sands, which begins at current velocities between 0.90 m $s^{-1}$ to 1.60 m $s^{-1}$ in 3–5 cm water depths. Thus, in the present study, current velocity must be higher than the critical shear stress velocity for erosion of epibenthic microbial mats (1.60 m $s^{-1}$) that ripped the mats, exhibiting sharp edges (red arrow in Fig. 9F). We found similar erosional pockets documented by Noffke (1999) (Fig. 11D), but other depressions were formed by the ripped-up of the surficial microbial mat exposing old microbial mats exhibiting a flat surface (Fig. 9C, D, F). As a consequence of the high current velocity, the tearing of the superficial cohesive microbial mat over long distances occurred creating regularly large rolled-up mats over the tidal flat (Fig. 9D, E, G).

Two days after the storm event in June 2018, a long tear-mat was measured for 12 m, but the images from the UAV detect greater structures over the tidal flat (Video 1, Apendix A). A high frequency of large roll-ups presence over the channel zone was exhibited by UAV records. The surficial mat separated from the underlying water-saturated sediment has a slippery behavior under the current shear stress forming mat folds in different directions (Fig. 9F, G). Sometimes, not far from the mat fold, it is possible to identify the tear exposing the underlying sediment that generates the mat fold (Fig. 11C). Also, flipped-over mats are formed on the sharp borders of the

erosional pocket, exposing different directions. Otherwise, flipped-over mats were induced by pre-existing cracks (Fig. 7B) similarly to the estuarine environment under storm condition (Cuadrado et al., 2013; 2014).

*5.3. Mechanism of refilling the gas domes and mat folds*

The mat deformation structures such as gas domes and mat folds requires a thick epibenthic mat characterized by a high flexible behavior when is wet. In the case of the mat folds, it is essential a high shear stress exerted by water currents to tear and deform the mat after the sliding over the underlying sediment. The process of formation makes the lifting of the cohesive and waterproof microbial carpet (~1 cm in thickness), losing contact with the underlying sediment and generating a hollow center (Fig. 6C).

The characteristically high cohesiveness and low permeability of the mats and the water-saturated underlying sediments make an aquifer capped by microbial mats. The hydraulic pressure (uplift force) from the aquifer is superimposed by the hydrostatic pressure from the water column. It is important to take into account the continuous action of wind waves over the water column since the inundation occurs under storm conditions with strong winds.

The presence of an impermeable barrier, the microbial mat, increases the likelihood of underlying sand liquefaction by wave's action, as it leads to areas of increase pore-fluid pressure (Obermeier, 1996). This fact might cause two effects: 1) a mat detachment triggered by the air due to the rising groundwater table before mentioned; 2) the pore-fluid overpressure plus the groundwater movement under a persistent wave action of the water column induce the liquefaction of the underlying sand (Owen and Moretti, 2011). Thus, the internal friction of sediment is reduced to nearly zero, and the material act temporarily as a fluid. If the surficial microbial mat had been deformed detached from

the underlying sediment, the liquefaction produces the sand redistribution under the microbial mat adapting the deformation shape (Video 3, Appendix A). However, not all microbial domes and folds show sand filling-up the mat deformation (Fig. 6C). Liquidized sand may only occurs when long periods of water stay over the tidal flat (more than a day, showed in water-level records, Figs. 2, 3), in agreement with experiment results carried out on soft-sediment deformation by Owen and Moretti (2011) where the morphology of the deformed sediment depends on the duration of the liquefied state, among others.

### *5.5 Geomorphological factor*

The elongated morphology (more than 3 km in length) perpendicular to the coast, sheltered by a sandy spit, was transformed nowadays in a semi-closed extent protected from daily sea influence. Pulses of flooding alternating with calm periods give the mat the necessary conditions to form an epibenthic mat. Wind direction and speed undoubtedly help in driving the seawater into the zone during storms and consequently, flood currents enter in the prior morphology that accelerates the funneled water currents. So, strong currents are consequence of the coastal morphology. Therefore, in few hours there is a >0.50 m water depth over the tidal flat (Figs. 2F; 9A), where strong traction currents act over thick microbial mats. This fact indicates the relevance of the geomorphology, especially in specific microbial mat deformation such as great roll-ups mats. The geomorphology act in increasing current velocity creating MISS similarly as hurricane phenomenon as was indicated by Noffke (2010) in Portsmouth Island (USA).

## 6. **CONCLUSIONS**

Several MISS were documented in an inactive tidal channel in relation with hydrodynamics. The entering sea water percolates through the sediment, pushing air and gases through sedimentary pores forming gas domes at the surface. However, severe erosional processes form other MISS. Strong landward storms reinforced by spring water tides push sea water onto the area, and fast flood tidal currents were increased by the coastal geomorphology. Thus, severe storms can roll up several $m^2$ of mat. Associated microbial structures such as folds, and flipped-over edges were also found in relation to rip-off mats. Large erosional pockets and remnants were also documented on the margin of the area where sand was less colonized.

Some deformation structures such as folds and gas domes, characterized by a hollow under the mat, were refilled by sand. To explain that fact we proposed a mechanism of sand liquefaction due to the oscillating pore-fluid overpressure under the wavy water column that generates the sand acting temporarily as a fluid. That fact might move the sand to the cavity beneath the deformation mat.

The progradation stage that characterizes this area influences the episodic flooding that favor and enhances sediment microbial colonization. Thus, the geomorphology is an essential factor that develops fast water currents acting on the microbial surface. Paso Seco is a nice example for formation of MISS, especially large deformation microbial structures.



**Acknowledgements**

This research was supported by CONICET (grant PIP 2013 N°4061 and 2015 Nº302); SECYT-UNS (grant PGI 24/H138), UTN FRBB PID MSUTIBB0004476TC. We thank J. Pan and L.A. Raniolo for their assistance in the field work. L.M. was supported by a Fellowship from CONICET.

**References**

Andres, M. S., Reid, R. P., 2006. Growth morphologies of modern marine stromatolites: a case study from Highborne Cay, Bahamas. Sedimentary Geology 185, 319-328.

Bose, S., Chafetz, H.S., 2009. Topographic control on distribution of modern microbially induced sedimentary structures (MISS): a case study from Texas coast. Sedimentary Geology 213, 136-149.

Bose, S., Chafetz, H. S., 2011. Morphology and distribution of MISS: a comparison between modern siliciclastic and carbonate settings. Microbial mats in siliciclastic depositional systems through time. Special Publication 101. Tulsa. SEPM Society for Sedimentary Geology 3-14.

Chafetz, H. S., Buczynski, C., 1992. Bacterially induced lithification of microbial mats. Palaios 7, 277-293.

Cuadrado, D. G., Pan, J., 2018. Field Observations on the Evolution of Reticulate Patterns in Microbial Mats in a Modern Siliciclastic Coastal Environment. Journal of Sedimentary Research 88, 24-37.

Cuadrado, D.G., Bournod, C.N., Pan, J., Carmona, N.B., 2013. Microbially-induced sedimentary structures (MISS) as record of storm action in supratidal modern estuarine setting. Sedimentary Geology 296, 1-8.

Cuadrado, D. G., Perillo, G. M., Vitale, A. J., 2014. Modern microbial mats in siliciclastic tidal flats: evolution, structure and the role of hydrodynamics. Marine Geology 352, 367-380.

Cuadrado, D. G., Pan, J., Gómez, E. A., Maisano, L., 2015. Deformed microbial mat structures in a semiarid temperate coastal setting. Sedimentary Geology 325, 106-118.

Decho, A. W., Gutierrez, T., 2017. Microbial extracellular polymeric substances (EPSs) in ocean systems. Frontiers in microbiology. doi: 10.3389/fmicb.2017.00922.

Ferrelli, F., Bohn, V.Y., Piccolo, M.C., 2012. Variabilidad de la precipitación y ocurrencia de eventos secos en el sur de la provincia de Buenos Aires (Argentina). IX Jornadas Nacionales de Geografía Física, Bahía Blanca, Argentina, pp. 15-28.

Gerdes, G., Krumbein, W.E., Noffke, N., 2000. Microbial signatures in peritidal siliciclastic sediments: a catalogue. Sedimentology 47, 279-308.

Gerdes, G., 2007. Structures left by modern microbial mats in their host sediments. In: Atlas of microbial mat features preserved within the siliciclastic rock record. Elsevier, Amsterdam, pp. 5-38.

Iglesias, A., 1981. Temperaturas. In: Chiozza, E., Figueira, R. (Eds.), Atlas Total de la República Argentina. Centro Editor de América Latina, Buenos Aires, pp. 204-208.

Kremer, B., Kazmierczak, J., Stal, L. J., 2008. Calcium carbonate precipitation in cyanobacterial mats from sandy tidal flats of the North Sea. Geobiology 6, 46-56.

Noffke, N., 1999. Erosional remnants and pockets evolving from biotic–physical interactions in a Recent lower supratidal environment. Sedimentary Geology 123, 175-181.

Noffke, N., 2010. Microbial Mats in Sandy Deposits from the Archean Era to Today. Springer-Verlag, Berlin, pp. 200.

Noffke, N., Paterson, D., 2008. Microbial interactions with physical sediment dynamics, and their significance for the interpretation of Earth's biological history. Geobiology 6, 1-4.

Noffke, N., Gerdes, G., Klenke, T., Krumbein, W.E., 2001. Microbially induced sedimentary structures-a new category within the classification of primary sedimentary structures. Journal of Sedimentary Research 71, 649-656.

Noffke, N., Beukes, N., Bower, D., Hazen, R.M., Swift, D.J.P., 2008. An actualistic perspective into Archean worlds- (cyano-) bacterially induced sedimentary structures in the siliciclastic Nhlazatse Section, 2.9 Ga Pongola Supergroup, South Africa. Geobiology 6, 5-20.

Obermeier, S.F., 1996. Use of liquefaction-induced features for paleoseismic analysis. Engineering Geology 44, 1-76.

Owen, G., Moretti, M., 2011. Identifying triggers for liquefaction-induced soft-sediment deformation in sands. Sedimentary Geology 235, 141-147

Pan, J., Cuadrado, D.G., Bournod, C.N., 2017. Diatom-driven colonization of microbial mat-dominated siliciclastic tidal flat sediments. FEMS Microbiology Ecology 93, 1-13.

Schieber, J., 1999. Microbial mats in terrigenous clastics: the challenge of identification in the rock record. Palaios 14, 3-12.

Schieber, J., 2004. Microbial Mats in the Siliciclastic Rock Record: A Summary of Diagnostic Features. In: Eriksson, P.G., Altermann, W., Nelson, D., Mueller, W.U., Catuneanu, O., Strand, K. (Eds.), The Precambrian Earth: Tempos and Events, Developments in Precambrian Geology. Elsevier, pp. 663-672.

Stal, L., 2012. Cyanobacterial mats and stromatolites. In: Whitton, B.A. (Eds.), Ecology of Cyanobacteria II: Their Diversity in Space and Time. Springer, Netherlands, pp. 65-125.

**Figure captions**

Fig. 1. Location of study area. (A) Colonized area by microbial mat is delineated. HS is the Hobo station location. (B) Oblique photograph of the narrow passage where the sea water enter the study zone. The sea can be seen at the background.

Fig. 2. Water level records. (A) 2-years record (from March 2015 to March 2017). The mat tidal flat surface is indicated by a red line. (B) Variation in water level from March 20$^{th}$ to April 25$^{th}$, 2015. The arrow indicates a rainy event that replenished the aquifer. (C) Water column from March 20$^{th}$ to March 31$^{th}$, 2015. (D) Variation in water level from April 1$^{st}$ to April 3$^{rd}$, 2015. (E) Variation in water level from April 20$^{th}$ to April 22$^{nd}$, 2015. The arrow indicates the moment the surficial current velocity was measured (0.50 m s$^{-1}$) during the field survey. (F) Variation in water level from May 2$^{nd}$ to May 6$^{th}$, 2015, when the highest column water was reached.

Fig. 3. Variation in water level during austral winter and summer. (A) During June 2015. (B) From June 1$^{st}$ to August 10$^{th}$, 2016. (C) November and December 2015. (D) January and February, 2017.

Fig. 4. Seasonally appearance of the microbial tidal flat. (A) Photograph taken in July 2015 after the highest inundation in the period. Dashed line indicates mat fragments at the vegetation border pointing out the water level that had affected the area. (B) Close view of mat fragments on the vegetation. (C) Large mat fragment over the vegetation ripped form the microbial tidal flat and deposited on the vegetated border. (D) Appearance of the tidal flat during winter where the water table is close to the tidal flat. (E) Appearance of the tidal flat during summer showing a dry aspect. (F) Close view of a desiccation crack on the surface tidal flat in summer. The subsurface of the mat remained moistly.

Fig. 5. (A) Surficial mat showing the geochemical conditions represented by an oxic zone at the top and an anoxic zone with a black colour below. The planar lamination can be seen in the anoxic layer. (B) "Crinkle coating" in the surficial mat above the oxic layer. There is a very thin green cyanobacteria-lamina below. (C) Cross-vertical section of a sediment core showing a biolaminite, microbial mat laminae intercalated by sandy layers. Darker layers present a sandy/silt composition and lighter layers are identified as microbial mat (see text for details). At the bottom the old microbial mats present a curvature (pointed by an arrow).

Fig. 6. Gas dome structure. (A) A dome structure appearing above the water level (under windy conditions that create small waves) during the flooding of the tidal flat with a circular shape in plane. Water depth ~10 cm. (B) Dome structures ~9 cm in diameter with a circular shape in plane. (C) Profile of a dome structure showing a hollow below. (D) Under dry condition, covered by pinnacles. The underlying bedding presents the same shape of the surficial mat dome.

Fig.7. Flipped-over edges. (A) The thick mat was torn and flipped over containing part of the underneath sediment (rough appearance). (B) Flipped-over edges developed by the ebb currents. The rose diagram (n=24) shows the ebb direction in relation to the longitudinal orientation of the channel (red arrow indicates flood direction).

Fig. 8. (A) Recumbent fold with the axial plane oriented at low angle with the horizontal tidal flat. (B) Wet mat fold exposed near a mat tear. (C) Close view of the thick mat forming the fold with sand sediment below fitting the deformation. (D) Mat roll-up structure formed by the winding of a long mat tear. There were flipped-over edges associated with a roll-up structure (FO). (E) Close view of a mat fragment which has been rolled over.

Fig.9. (A) Water level record of a storm in June 2018, two days before a field trip. (B) Erosional pocket formed by the high energy of the previous storm. Two people for scale. (C) Long mat tears (T) ending in roll ups (RU). The sediment transport (ST) along the ancient channel is showed. A person is rounded. (D) Mat deformation structures after the storm: mat tears (T), roll ups (RU) and folds (F). (E) Close view of the mat roll up. (F) Mat deformation associated to a ripped mat (T): fold over (yellow arrows), mat fold formed by the slippery behaviour of the mat (white arrow), and thick border of the tear (red arrow). (G) Tidal flat aspect covered by a thin sheet of water (5 cm deep), showing the mat deformation structures: mat folds (F) and roll ups (RU). A person is rounded.

Fig. 10. (A) Ancient tidal orientation pointed by an arrow (226°N). (B) (C) Rose diagram showing mat tear (B) and mat roll up (C) orientation in relation to the flood direction (red arrow).

Fig. 11. Mat deformation structures 46 days after the severe storm. (A) Mat roll up created after the mat was ripped off associated to the flood direction. (B) Mat ripped off forming a roll up in flood direction. Fold over mat (yellow arrow) at the border of the tear. Sharp borders (white arrows) can be seen showing different planar old mats. Sediment transport is shown (red arrow). (C) A mat fold creation (white arrows) after the separation of a mat tear (black arrow) and the gliding movement over the underlying sediment. (D) Erosional pocket in relation to the longitudinal orientation of the area.

Fig. 12. Recolonization. (A) The yellow-colour aspect in R shows the recolonization by microorganism. (B) Flipped-over edge which is being recolonized by cyanobacteria filaments. The cyanobacteria are forming reticules on the top of the structure and also in the borders (arrow). (C) Edges of a mat fold structure became diffuse forming part of a new sedimentary layer (arrows).

Fig. 13. (A) A vertical section of an erosional flank of a tidal channel that crosses the mat tidal flat, where lamination and a microbial deformed structure can be appreciated (white arrow). The surficial and dried microbial mat covers the underlying biolaminite (black arrow). (B) A rigid desiccated microbial small dome extracted from the surface tidal flat. (C) A cross-vertical section of a sedimentary core. A deformed structure can be identified at the bottom, 13 cm in depth (white arrow).

**Supplementary data. Appendix A.**

Video 1. Video obtained two days after a severe storm occurred on the study area. Several deformed structures were created by strong water currents that reached 0.70 m column water (see Fig. 10A). Several tears and roll ups can be identified.

Video 2. The sea water entering the study area lifts a piece of mat which is separating from the microbial surface. The current velocity might be appreciated by the pieces of floating vegetation on the water surface.

Video 3. The sand below the microbial fold has the same morphology of the mat due to the liquefaction process during an inundation for more than a day (see text for details). The sand is covered by very fine sediment. The very flexible microbial mat has a ~1 cm thickness.

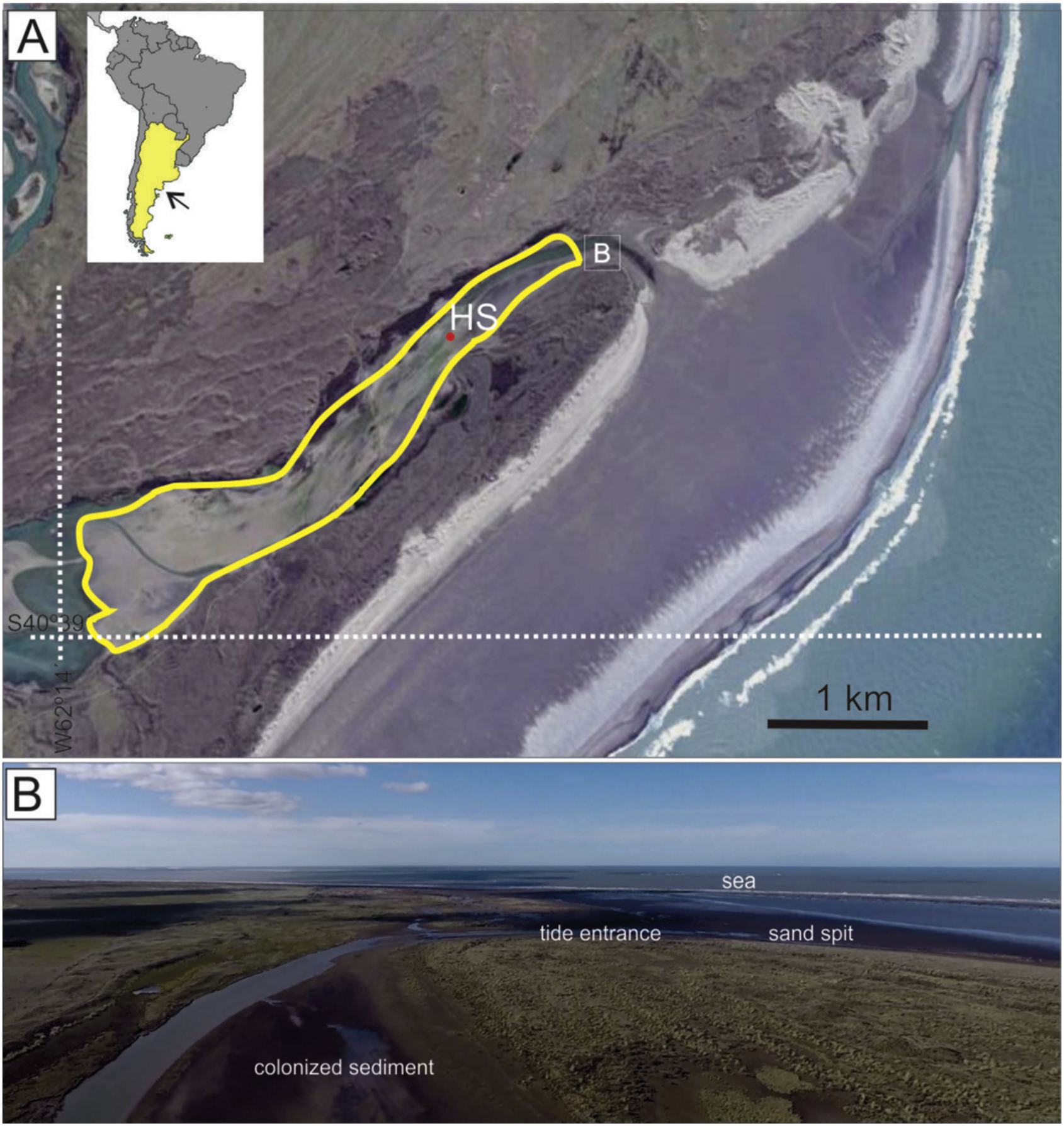
A
B
HS
S40°39'
W62°14'
1 km
B
sea
tide entrance
sand spit
colonized sediment

Figure 1

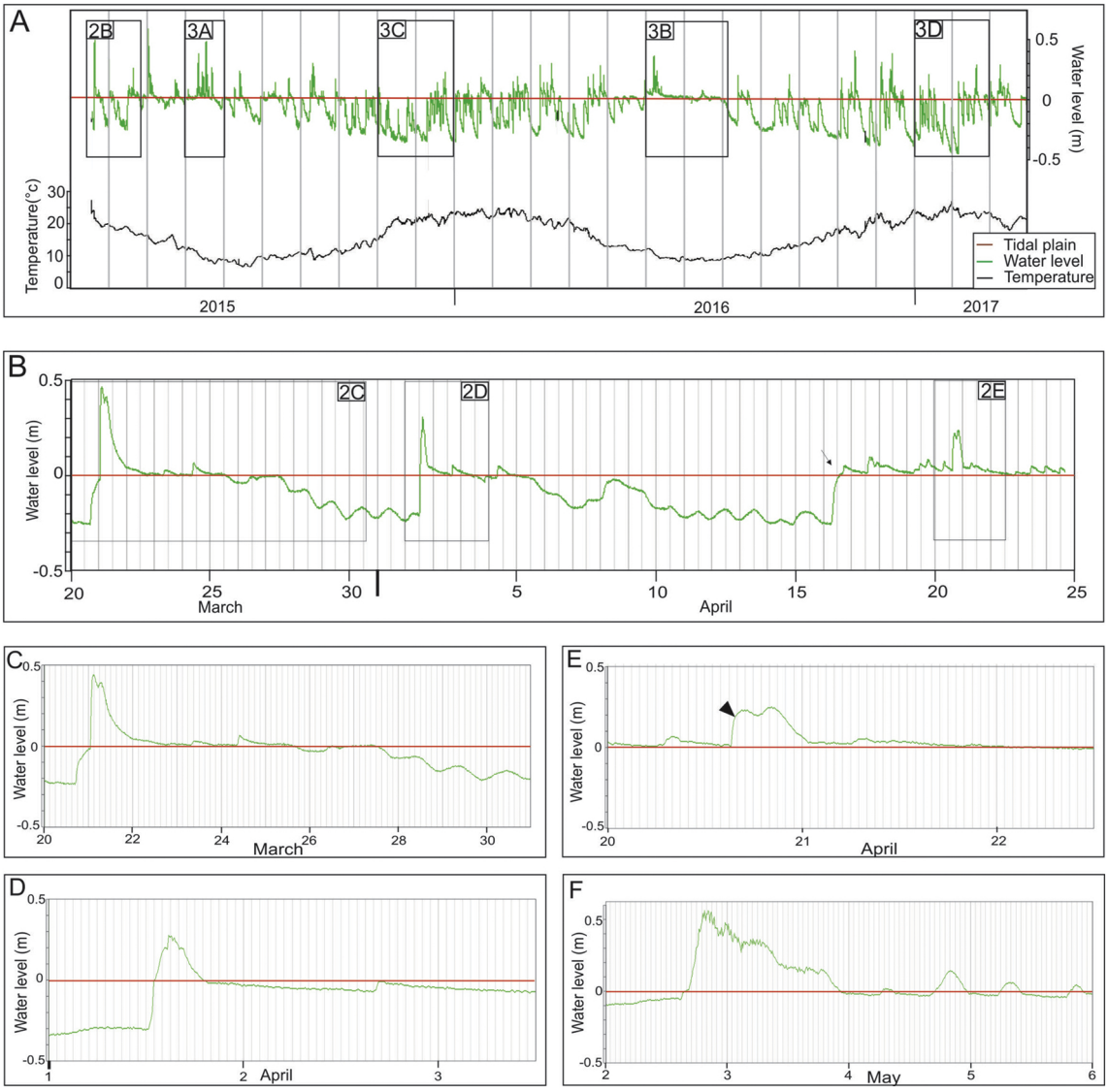
A
2B
3A
3C
3B
3D
Water level (m)
0.5
0
-0.5
Temperature(°c)
30
20
10
0
Tidal plain
Water level
Temperature
2015
2016
2017
B
2C
2D
2E
Water level (m)
0.5
0
-0.5
20
25
30
March
5
10
15
20
25
April
C
Water level (m)
0.5
0
-0.5
20
22
24
26
28
30
March
E
Water level (m)
0.5
0
-0.5
20
21
22
April
D
Water level (m)
0.5
0
-0.5
1
2
April
3
F
Water level (m)
0.5
0
-0.5
2
3
4
May
5
6

Figure 2

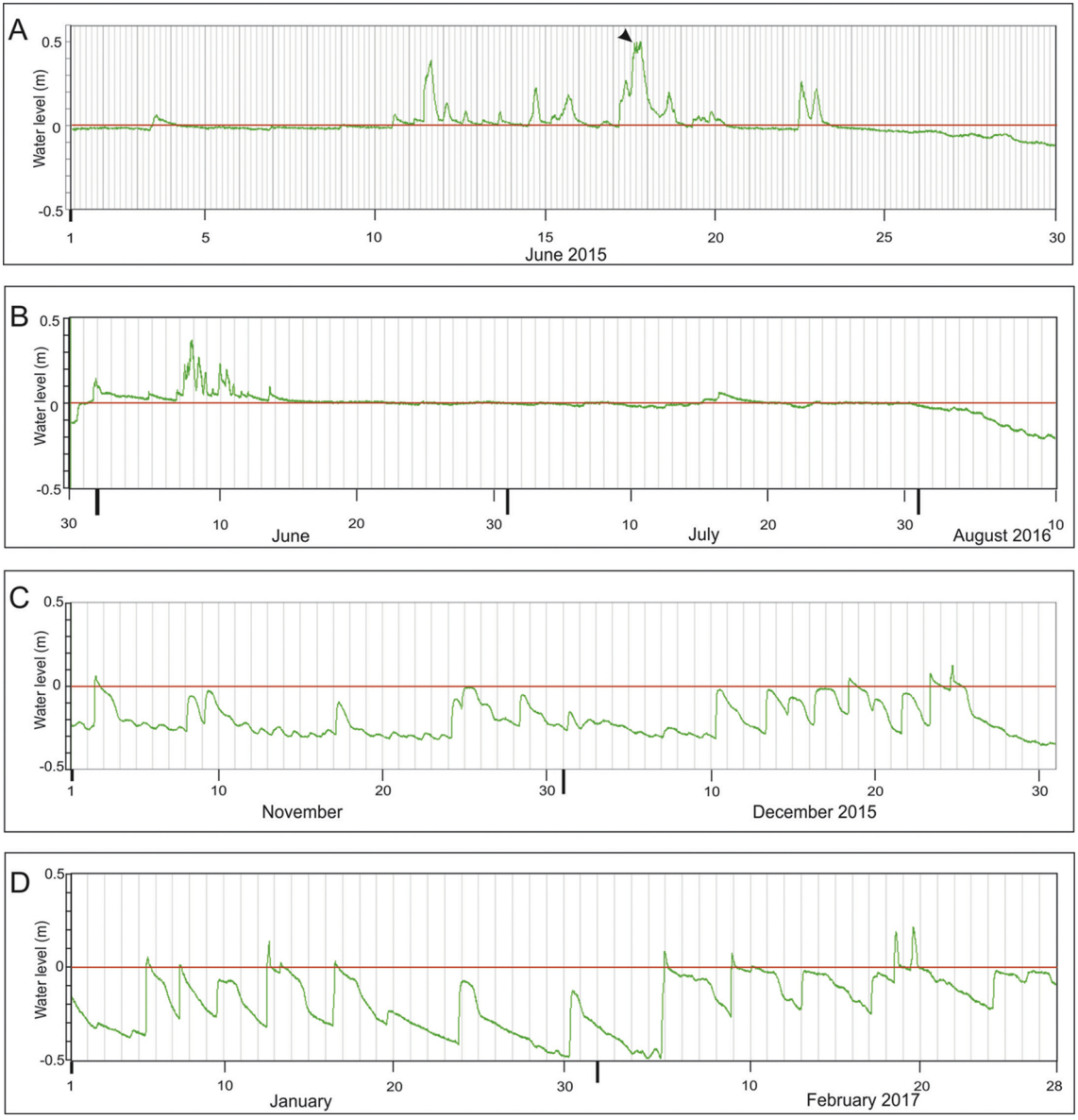
A
Water level (m)
0.5
0
-0.5
1
5
10
15
20
25
30
June 2015
B
Water level (m)
0.5
0
-0.5
30
10
June
20
30
10
July
20
30
August 2016
10
C
Water level (m)
0.5
0
-0.5
1
10
20
30
November
10
20
30
December 2015
D
Water level (m)
0.5
0
-0.5
1
10
20
30
January
10
20
28
February 2017

Figure 3